

Flow about a fluid sphere at low to moderate Reynolds numbers

By D. L. R. OLIVER† AND J. N. CHUNG

Department of Mechanical Engineering, Washington State University,
Pullman, WA 99164-2920, USA

(Received 18 July 1986)

The steady-state equations of motion are solved for a fluid sphere translating in a quiescent medium. A semi-analytical series truncation method is employed in conjunction with a cubic finite-element scheme. The range of Reynolds numbers investigated is from 0.5 to 50. The range of viscosity ratios is from 0 (gas bubble) to 10^7 (solid sphere). The flow structure and the drag coefficients agree closely with the limited available experimental measurements and also compare favourably with published finite-difference solutions. The strength of the internal circulation was found to increase with increasing Reynolds number. The flow patterns and the drag coefficient show little variation with the interior Reynolds number. Based on the numerical results, predictive equations for drag coefficients are recommended for both moderate- and low-Reynolds-number flows.

1. Introduction

The literature contains numerous theoretical solutions for flow over a solid sphere and a gas bubble. In both of these cases, the internal circulation may be neglected with the no-slip or no-shear stress boundary conditions respectively. Clift, Grace & Weber (1978), present a good review of previous work in this area.

For a fluid droplet where the viscosity ratio is not near one of these extremes (that of a solid sphere or a gas bubble), the additional internal flow field must be solved simultaneously. Both Hadamard (1911) and Rybczynski (1911) independently presented solutions for steady flows inside and around an axisymmetric fluid sphere with the creeping-flow assumptions. In the 1960s, several attempts were made using a Galerkin approach to solve for the flow field with the nonlinear convective terms included. A typical example is that presented by Nakano & Tien (1967). These Galerkin solutions did not contain enough terms to accurately describe the flow field at moderate Reynolds numbers. They also did not contain the correct trial functions to converge to the solution of Hadamard and Rybczynski at low Reynolds numbers. (For this study, unless otherwise indicated, the Reynolds number is based on the exterior properties.)

In the 1970s several finite-difference models were presented: LeClair *et al.* (1972) were the first to use a finite-difference method to calculate the steady motion of water drops in air. Their numerical results compare favourably with their own wind-tunnel measurements. Predictive equations are presented in Abdel-Alim & Hamielec (1975) and Rivkind, Ryskin & Fishbein (1976) to estimate the drag coefficient as a function

† Present address: Department of Mechanical Engineering, University of Toledo, Toledo, OH 43606, USA.

of both the viscosity ratio X (interior to exterior) and the Reynolds number. Abdel-Alim & Hamielec (1975) proposed the following equation for the drag coefficient:

$$C_d = 26.5 Re_{\text{ex}}^{-0.74} \left[\frac{(1.3 + X)^2 - 0.5}{(1.3 + X)(2.0 + X)} \right].$$

Re_{ex} is defined as
$$Re_{\text{ex}} = \frac{2Ua}{\nu_{\text{ex}}},$$

where U is the free-stream velocity, a is the drop radius, and ν_{ex} is the exterior kinematic viscosity. Rivkind & Ryskin (1976) proposed another equation to estimate the theoretical drag coefficient on such a drop:

$$C_d = \frac{1}{1 + X} \left[X \left(\frac{24}{Re_{\text{ex}}} + 4 Re_{\text{ex}}^{-\frac{1}{2}} \right) + 14.9 Re_{\text{ex}}^{-0.78} \right].$$

A quick comparison demonstrates that differences of up to 20% may occur between these two equations (for $Re_{\text{ex}} \leq 20$). In addition to the above discrepancy, as the Reynolds number approaches zero neither of the above equations approach the drag coefficients predicted by the Hadamard and Rybczynski solution: $C_{d\text{cr}} = 16[(1 + 1.5X)/(1 + X)]/Re_{\text{ex}}$.

In a recent paper, Oliver & Chung (1985) investigated the steady flows inside and around a fluid sphere at low Reynolds numbers by a hybrid method of the series-truncation technique and the finite-difference numerical approximation. They found that the density difference between the fluid sphere and its ambient fluid has almost no effect on the drag coefficient at low Reynolds numbers. The shear stress and the drag coefficient increase with increasing viscosity ratio of fluid sphere to ambient fluid and decrease with increasing Reynolds number.

Brabston & Keller (1975) used the same hybrid method to study the flow around a gas bubble. Their results show that the calculated drag coefficients compare well with those obtained by asymptotic analysis for high-Reynolds-number flow when the Reynolds number is greater than 40 and also agree with creeping-flow solutions if the Reynolds number is smaller than 0.5.

Instead of a finite-difference method, the combination of the series-truncation and a cubic finite-element scheme are selected in this paper for predicting the flows inside and around a fluid sphere at low to moderate Reynolds numbers. It is intended to demonstrate the feasibility of this new technique and some novel features of this hybrid method for solving highly nonlinear flows. It is also intended to independently calculate the flow fields using a method that incorporates no finite-difference methods and then to determine what causes the discrepancy between the results of Abdel-Alim & Hamielec (1975) and Rivkind & Ryskin (1976) as mentioned above. More importantly, there seems to be a lack of information on the fluid mechanics of a drop in the moderate-Reynolds-number range of 1 to 100. Existing analytical solutions (mostly asymptotic methods) are only applicable to extremely small (< 1) or large (> 100) Reynolds numbers. Most of the experimental investigations in the literature deal with Reynolds numbers larger than 100. Also all experimental results carry some uncertainties due to certain degrees of surface contamination, which explains the wide range of variations in reported experimental findings.

The assumptions used in this work are identical with those used in Oliver & Chung (1985). Owing to the larger Reynolds numbers investigated in this work, it should be emphasized that a steady, axisymmetrical, laminar solution is sought.

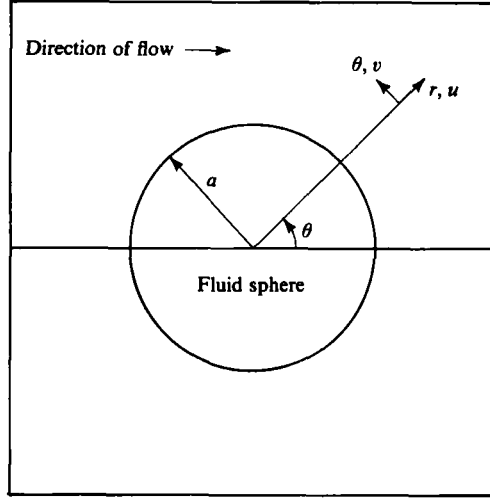


FIGURE 1. Coordinate system.

2. Mathematical formulation

A fluid sphere with density ρ_{in} , viscosity μ_{in} is translating in continuous fluid with density ρ_{ex} and viscosity μ_{ex} . The coordinate system is such that the origin is fixed to the droplet centre and $\theta = 0$ is directed downstream, see figure 1.

The equation of continuity is satisfied by introducing the dimensionless stream function ψ , defined by the dimensionless velocities

$$u = \frac{1}{r^2 \sin \theta} \frac{\partial \psi}{\partial \theta}, \quad v = \frac{-1}{r \sin \theta} \frac{\partial \psi}{\partial r}. \quad (1)$$

The stream function is made dimensionless with Ua^2 , where a is the radius of the droplet; the velocities are made dimensionless with the free-stream velocity U . The dimensionless radial coordinate r is made dimensionless by a .

The dimensionless equation of motion in terms of the stream function is

$$D^4 \psi = \frac{1}{2} \sin \theta \operatorname{Re} \left[\frac{\partial \psi}{\partial r} \frac{\partial}{\partial \theta} \left(\frac{E^2 \psi}{r^2 \sin^2 \theta} \right) - \frac{\partial \psi}{\partial \theta} \frac{\partial}{\partial r} \left(\frac{E^2 \psi}{r^2 \sin^2 \theta} \right) \right], \quad (2)$$

with

$$D^2 = \frac{\partial^2}{\partial r^2} + \frac{\sin \theta}{r^2} \frac{\partial}{\partial \theta} \left(\frac{1}{\sin \theta} \frac{\partial}{\partial \theta} \right).$$

Equation (2) is valid for both the fluid sphere and its ambient flow. Re should be $Re_{in} = 2\rho_{in} Ua/\mu_{in}$ for flow in the fluid sphere and $Re_{ex} = 2\rho_{ex} Ua/\mu_{ex}$ for ambient flow.

The boundary conditions to be satisfied by (2) are

(i) At the axis symmetry ($\theta = 0, \pi$):

$$\frac{\partial \psi_{in}}{\partial \theta} = 0 \quad (u \text{ is finite}), \quad (3)$$

$$\psi_{in} = 0 \quad (\text{arbitrary constant}). \quad (4)$$

(ii) At the interface ($r = 1$):

$$\frac{\partial \psi_{\text{in}}}{\partial r} = \frac{\partial \psi_{\text{ex}}}{\partial r} \quad (\text{no slip}), \quad (5)$$

$$\tau_{r\theta_{\text{in}}} = \tau_{r\theta_{\text{ex}}}, \quad (6)$$

$$\psi_{\text{in}} = \psi_{\text{ex}} = 0. \quad (7)$$

(iii) At free-stream conditions (r_∞):

$$\psi_{\text{ex}} = \frac{1}{2} r_\infty^2 \sin^2 \theta. \quad (8)$$

In the above, $\tau_{r\theta}$ is the interfacial shear stress.

3. Solution procedure

The series-truncation method used by Dennis & Walker (1971) for flow about a solid sphere is used in this analysis. It was also adopted by Brabston & Keller (1975) for flow about a gas bubble; that is, we define the stream function as an infinite series (later to be truncated) of associated Legendre functions P_n^l with corresponding unknown radial functions F_n . Equation (2) is transformed into a series of ordinary differential equations (in the radial direction). Specifically let

$$\psi = \sum_{n=1}^{\infty} F_n(r) \int_1^z P_n^l(t) dt; \quad z = \cos(\theta). \quad (9)$$

Then, using the orthogonality of these Legendre functions and the additional property

$$P_i^l(z) P_l^m(z) = (-1)^M \left[\frac{(l+m)! (i+j)!}{(l-m)! (i-j)!} \right]^{\frac{1}{2}} \times \sum_k^{\infty} (2k+1) \begin{pmatrix} i & l & k \\ j & m & -M \end{pmatrix} \begin{pmatrix} i & l & k \\ 0 & 0 & 0 \end{pmatrix} \left[\frac{(k-M)!}{(k+M)!} \right]^{\frac{1}{2}} P_k^M(z), \quad (10)$$

with $M = j + m$.

The coefficients

$$\begin{pmatrix} i & j & k \\ l & m & n \end{pmatrix}$$

are the '3- J ' symbols. Talman (1968) presents the theory of these coefficients with respect to associated Legendre functions. Rottenberg *et al.* (1959), review several useful relations used for calculating these coefficients.

After much manipulation, (2) is converted, via (10) and the orthogonality of Legendre functions, to

$$\frac{-F_n^{\text{iv}}}{n(n+1)} + \frac{2F_n''}{r^2} - \frac{4F_n'}{r^3} + [6 - n(n+1)] \frac{F_n}{r^4} - S_n = 0, \quad (11)$$

with

$$S_n = \frac{1}{2} \text{Re} \sum_{i,j}^{\infty} \left[CU_{i,j}^n F_i \left(\frac{-F_j''}{r^{2j}(j+1)} + \frac{2F_j''}{r^{3j}(j+1)} + \frac{F_j'}{r^4} - \frac{4F_j}{r^5} \right) + CV_{i,j}^n F_i' \left(\frac{-F_j''}{r^{2j}(j+1)} + \frac{F_j}{r^4} \right) \right],$$

where Re is the appropriate Reynolds number (Re_{in} or Re_{ex}). The primes indicate differentiation with respect to r and the coefficients CU and CV are given by

$$\left. \begin{aligned} CU_{i,j}^n &= -(2n+1) \left[\frac{j(j+1)}{n(n+1)} \right]^{\frac{1}{2}} \begin{pmatrix} n & i & j \\ -1 & 0 & 1 \end{pmatrix} \begin{pmatrix} n & i & j \\ 0 & 0 & 0 \end{pmatrix}, \\ CV_{i,j}^n &= (2n+1) \left[\frac{j(j^2-1)(j+2)}{n(n+1)i(i+1)} \right]^{\frac{1}{2}} \begin{pmatrix} n & i & j \\ -1 & -1 & 2 \end{pmatrix} \begin{pmatrix} n & i & j \\ 0 & 0 & 0 \end{pmatrix}. \end{aligned} \right\} \quad (12)$$

The transformed boundary conditions become

(i) At the sphere centre ($r = 0$):

$$F'_{n_{in}}(0) = 0, \quad (13)$$

$$F_{n_{in}}(0) = 0. \quad (14)$$

(ii) At the interface ($r = 1$):

$$F'_{n_{in}}(1) = F'_{n_{ex}}(1), \quad (15)$$

$$X(-F''_{n_{in}} + 2F'_{n_{in}}) - (-F''_{n_{ex}} + 2F'_{n_{ex}}) = 0, \quad (16)$$

$$\begin{aligned} F_{n_{in}}(1) &= F_{n_{ex}}(1) \\ &= 0. \end{aligned} \quad (17)$$

(iii) At the free stream ($r = r_\infty$):

$$F_{n_{ex}}(r_\infty) = r_\infty^2 \delta_{n1}, \quad (18)$$

$$F'_{n_{ex}}(r_\infty) = 2r_\infty \delta_{n1} \quad (\delta_{ij} = \text{Kronecker delta function}). \quad (19)$$

Equation (11) represents an infinite system of coupled ordinary differential equations. The order of equations is made finite by truncation of the series in (9); that is, we set all $F_n(r) = 0$, for $n > n_0$. The value of n_0 at which the omitted terms have an insignificant effect on the solution is found by trial and error. At low Reynolds number, only a very few terms are needed for good convergence owing to the relative symmetry about $\theta = \frac{1}{2}\pi$ of low-Reynolds-number flows. However, as the convective terms become more important, this symmetry is destroyed and more terms are needed in the truncated series for adequate convergence of the series.

The truncated form of (11) is solved numerically by finite-element methods where the domain is divided into several elements (generally five interior and 11 exterior elements). The trial functions used are cubic Hermite polynomials with C^1 continuity. See Huebner (1975) for a good explanation of these polynomials as they relate to finite-element interpolation functions.

Each cubic element corresponds to four interpolation functions, ' N_i ' (see Huebner 1975):

Interpolation function	Corresponding node
$N_1 = 1 - 3s^2 + 2s^3$	1
$N_2 = (\Delta r) s(s-1)^2$	1
$N_3 = s^2(3-2s)$	2
$N_4 = (\Delta r) s^2(s-1)$	2,

with $s = (r - r_0)/(r_1 - r_0)$, and $\Delta r = r_1 - r_0$. The node and element labelling schemes are shown in figure 2. The schematic diagram of the C^1 cubic Hermite-polynomials representation for an element is given in figure 3.

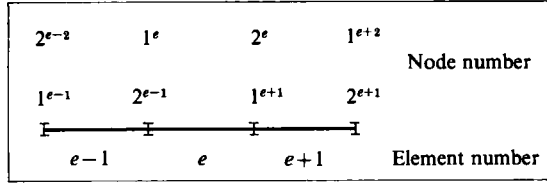
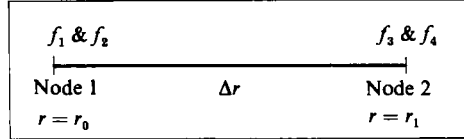


FIGURE 2. Node/element labelling scheme.

FIGURE 3. Representation of an element using C^1 cubic Hermite polynomials for trial functions.

Equation (11) in its truncated form represents n_0 equations over the entire domain $0 < r < r_\infty$. These n_0 equations are transformed into $4n_0$ equations for each element by employing Galerkin's method for each element; that is, (11) is multiplied by each of the four interpolation functions N_i and then integrated over each of the elemental domains:

$$\int_{r_0}^{r_1} N_i \left(\frac{-F_n^{iv}}{n(n+1)} + \frac{2F_n''}{r^2} + \dots - S_n \right) dr = 0. \quad (20)$$

Note that

$$\int_{r_0}^{r_1} -F_n^{iv} N_i dr = \int_{r_0}^{r_1} -F_n'' N_i'' dr - [N_i F_n''' + N_i' F_n''] \Big|_{r_0}^{r_1}, \quad (21)$$

$$\int_{r_0}^{r_1} \frac{F_j F_k'''}{r^2} N_i dr = \frac{F_j F_k''}{r^2} N_i \Big|_{r_0}^{r_1} - \int_{r_0}^{r_1} F_k'' \left[\frac{F_j N_i}{r^2} \right]' dr. \quad (22)$$

Define the vectors

$$\phi_{n,i}^e = \int_{r_0}^{r_1} \left\{ \frac{-F_n'' N_i'}{n(n+1)} + \left[\frac{2F_n''}{r^2} + \dots - (S_n - T_n) \right] N_i \right\} dr - \int_{r_0}^{r_1} \frac{1}{2} Re \sum_{j,k} \frac{C U_{i,j}^n}{k(k+1)} F_k'' \left(\frac{F_j N_i}{r^2} \right)' dr, \quad (23)$$

$$d_{n,i}^e = \frac{N_i F_n''' - N_i' F_n''}{n(n+1)} \Big|_{r_0}^{r_1} - \frac{1}{2} Re \sum_{j,k} C U_{j,k}^n \left[\frac{F_j F_k'' N_i}{k(k+1)r^2} \right] \Big|_{r_0}^{r_1}, \quad (24)$$

where the superscript e denotes element e and where

$$T_n = -\frac{1}{2} Re \sum_{j,k} C U_{j,k}^n F_j \frac{F_k''}{k(k+1)r^2}.$$

Using the above vector representations, (11) becomes, in vector form,

$$\phi_{n,i}^e = d_{n,i}^e. \quad (25)$$

The variable F_n is approximated on each elemental domain by the discrete approximation

$$F_n \approx \sum_{i=1}^4 f_{n,i}^e N_i. \quad (26)$$

The elemental systems of equations plus the appropriate boundary equations are combined into a global system of equations. This global system is linearized using a Newton iterative scheme. With proper arrangement, this global system has a block tridiagonal form with each block being a $2n_0 \times 2n_0$ submatrix. With such a block tridiagonal system, the number of calculations per iteration is roughly proportional to En_0^3 , where E is the total number of elements.

This iterative solution procedure is quite efficient at lower Reynolds numbers where only a few terms are required for good convergence. As the convective terms become more important, the flow field becomes quite asymmetric (about the $\theta = \frac{1}{2}\pi$ axis) and increasingly more terms are needed. For this reason, this investigation employs up to $n_0 = 20$ for $Re_{ex} = 50$.

The global Newton system of equations was iterated until convergence was attained. Convergence was assumed when the drag coefficient C_d ceased to change; that is, convergence was assumed when

$$\left| \frac{C_d^{\text{old}}}{C_d^{\text{new}}} - 1 \right| \leq 0.001,$$

where C_d^{old} and C_d^{new} are the previous and the updated drag coefficients respectively.

The drag coefficient is defined as

$$C_d = \frac{\text{Drag}}{\frac{1}{2}\rho_{ex} U^2 a^2 \pi}. \quad (27)$$

The drag is often separated into two components: the form drag and the viscous drag. These two components of the drag may be shown to be

$$\left. \begin{aligned} \text{Drag}_f &= -2\pi a^2 \int_0^\pi P \cos \theta \sin \theta \, d\theta, \\ \text{Drag}_v &= 2\pi a^2 \int_0^\pi (-\tau_{r\theta} \sin^2 \theta + \tau_{rr} \cos \theta \sin \theta) \, d\theta, \end{aligned} \right\} \quad (28)$$

where the subscripts v and f denote the viscous and form components, and where P is the pressure and $\tau_{r\theta}$ and τ_{rr} are tangential and normal stress tensors respectively. The parameters used in (28) (i.e. pressure, etc.) are measured on the exterior surface of the sphere.

One may show that the resulting components of the drag coefficient are given as

$$C_{df} = \frac{16}{3 Re_{ex}} \left(-\frac{1}{2} F_1''' + F_1' \right) + 8 \sum_{i=1}^{n_0} \frac{F_i' F_{i+1}'}{(2i+3)(i+1)(2i+1)}, \quad (29)$$

$$C_{dv} = \frac{16}{3 Re_{ex}} F_1''. \quad (30)$$

All derivatives have been evaluated on the exterior surface of the sphere. The total drag is merely the sum of the two components; hence, the total drag coefficient C_d is

$$C_d = C_{df} + C_{dv}. \quad (31)$$

4. Results and discussion

Determining the value at which the truncation is reasonable is an iterative process. As an example of the convergence of the solution with n_0 , the calculated drag coefficients are tabulated in table 1 for the special cases of $X = 0.333$ and 3.0 for

n_0	$X = 0.333$		$X = 3.0$	
	$Re = 1$	$Re = 50$	$Re = 1$	$Re = 50$
2	20.5	1.07	25.7	1.93
4	20.1	1.02	25.1	1.78
6	20.0	—	25.0	—
8	—	0.963	—	1.61
12	—	0.930	—	1.52
16	—	0.910	—	1.47
20	—	0.897	—	1.44

TABLE 1. C_d as a function of n_0 : ($Re_{in} = Re_{ex}$)

$Re_{ex} = 1.0$ and 50.0 . The convergence was rapid at low Reynolds numbers. However, at larger Reynolds numbers, the convergence with respect to n_0 was slow. For this reason, this solution procedure is considered quite efficient at lower Reynolds numbers, but requires extensive computation at moderate Reynolds numbers, a trend that is often associated with this type of nonlinear fluid-mechanics problem.

Another method of illustrating the convergence of the solution with respect to n_0 is by comparing the computed interfacial velocities as a function of n_0 . In figure 4 the interfacial velocities are plotted for a droplet with a viscosity ratio of $X = 3.0$ for Reynolds numbers of 1.0 and 50.0 , as a function of n_0 .

In addition to the convergence with respect to the infinite series it is also informative to investigate the convergence with respect to grid resolution and the location at which the free-stream conditions are assumed (r_∞). Two simulations were made using a coarser grid mesh and a smaller outer radius. Selected results are illustrated in table 2. The outer radii of the elements for both $r_\infty = 300$ and 100 are listed in table 3.

For larger values of viscosity ratio X , a recirculation region develops in the wake region. The flow field about the wake region has been studied experimentally by Taneda (1956) for solid spheres. As a check on the accuracy of the flow field predicted by this method, the recirculation region has been examined for a solid sphere ($X = 10^7$) for comparison with the experimental results of Taneda (1956). The flow lines about a solid sphere with $Re_{ex} = 30.0$ are plotted in figure 5.

At $Re_{ex} = 30.0$, the recirculation region in the wake is small. As the Reynolds number increases, the angle at which the recirculation region begins increases as does the length of the recirculation region. The outlines of the wake regions for $Re_{ex} = 30, 40$ and 50 are plotted in figure 6.

The distance from the location of the reattachment to the centre of the sphere has been estimated by Taneda (1956) using photographic means with a film of dried milk as a tracer. The radial position of the reattachment (as calculated by the present method) is compared with interpolations of the experimental results of Taneda (1956) in table 4. The agreement is excellent at $Re_{ex} = 30$; even at $Re_{ex} = 50$, the difference is still within the experimental errors.

The predicted drag coefficient is compared with the numerical (finite-difference) work of Rivkind & Ryskin (1976) in table 5. There is very good agreement between the two models for $Re_{ex} \leq 20$ (up to about 4% difference). The differences appear to be most pronounced at higher Reynolds numbers and for larger values of X . A check of the predicted drag coefficients calculated by the present method and the predictive

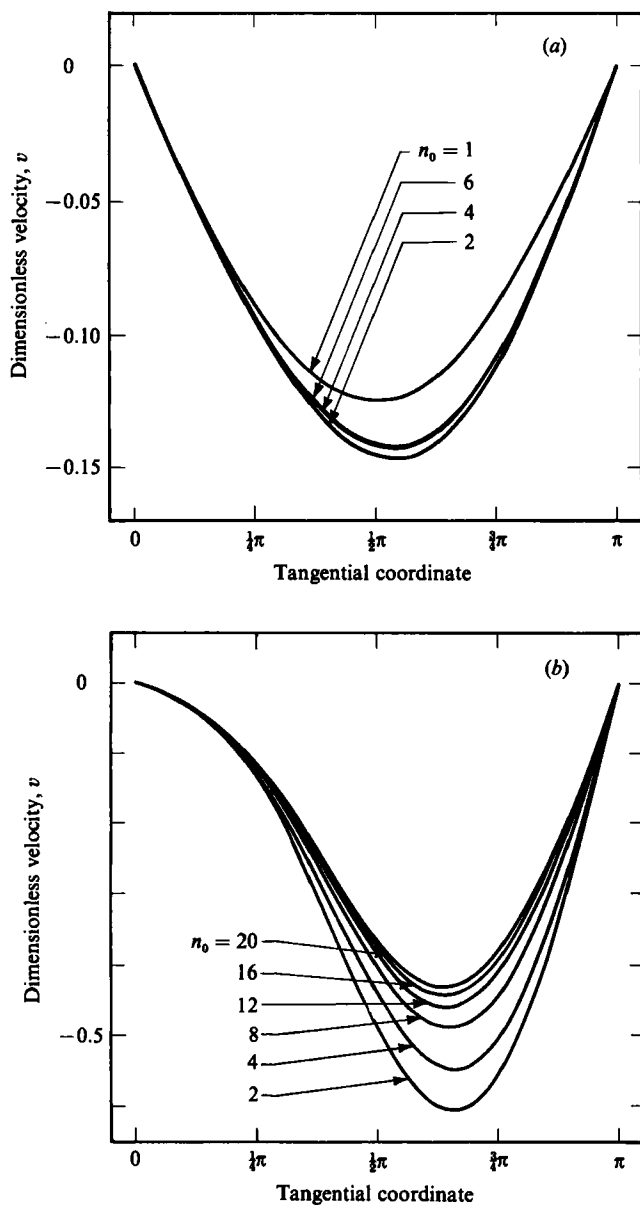


FIGURE 4. Tangential velocity at the interface as a function of n_0 for (a) $Re_{ex} = 1.0$, $X = 3.0$; (b) $Re_{ex} = 50.0$, $X = 3.0$.

equation proposed by Rivkind *et al.* (1976) indicates a good agreement for $2 \leq Re_{ex} \leq 20$. For $Re_{ex} = 50$, the present results exceed those of the Rivkind *et al.*'s (1976) predictive equation by up to 10%. Even though the disagreement is small, an attempt was made to compare these two numerical calculations with experimental data. Because of uncertainties concerning surface contamination and droplet deformation, it is meaningful only to compare the drag coefficients of solid spheres. The results of Elzinga & Banchemo (1961) were used because they are among the few experiments that cover the moderate-Reynolds-number range. The comparison is

	5 interior, 11 exterior elements $r_\infty = 300$	3 interior, 8 exterior elements $r_\infty = 100$
$Re = 1$	$C_d = 20.0$	$C_d = 20.0$
$X = 0.333$	$F'_1(1) = 0.833$ $F'_2(1) = -0.0855$	$F'_1(1) = 0.832$ $F'_2(1) = -0.0851$
$Re = 50$	$C_d = 1.44$	$C_d = 1.43$
$X = 3.0$	$F'_1(1) = 0.722$ $F'_2(1) = -0.541$	$F'_1(1) = 0.719$ $F'_2(1) = -0.540$

TABLE 2. Comparison of grid mesh sizes and r_∞ ($Re_{in} = Re_{ex}$)

$r_\infty = 300$		$r_\infty = 100$	
Element	Radius	Element	Radius
1	0.25	1	0.40
2	0.50	2	0.80
3	0.75	3	1.00
4	0.90	4	1.20
5	1.00	5	1.50
6	1.10	6	2.00
7	1.333	7	4.00
8	1.80	8	8.00
9	2.50	9	20.00
10	4.00	10	40.00
11	6.00	11	100.00
12	10.00		
13	20.00		
14	40.00		
15	100.00		
16	300.00		

TABLE 3. Outer radii of the elements

shown in table 6. It seems that the two different numerical methods converge to the experimental result from opposite directions for Re_{ex} at 50 but for lower Reynolds numbers the present calculations are closer to the results of Elzinga & Banchemo (1961).

The Elzinga & Banchemo (1961) experiments also included an ethylene glycol drop in finol which gives a Reynolds-number range of 30–80, $X = 0.9$ and $Re_{ex} = 0.75 Re_{in}$. They reported a drag coefficient of 1.25 for $Re_{ex} = 50$. Compared with 1.12 of Rivkind *et al.* (1976) and 1.15 of the present calculation for the case of $X = 1.0$, $Re_{ex} = 50$, and $Re_{ex} = Re_{in}$, the experimental result is high as expected owing to some surface contamination.

The computed drag coefficients may also be compared with the theoretical and experimental results of Abdel-Alim & Hamielec (1975). As mentioned above, there are wide ranges of experimental values for drag coefficients for fluid spheres in the

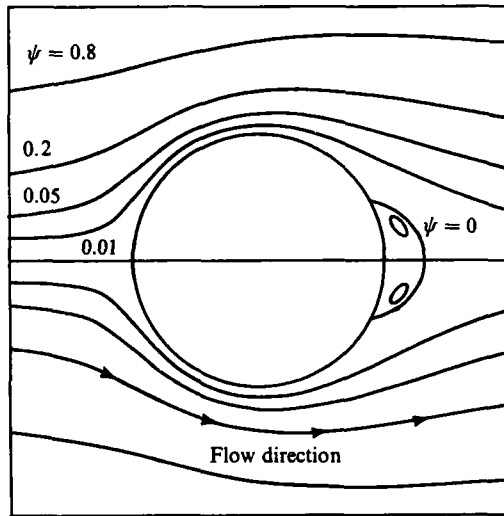


FIGURE 5. Stream-function contours, $Re_{ex} = 30.0$, $X = 10^7$.

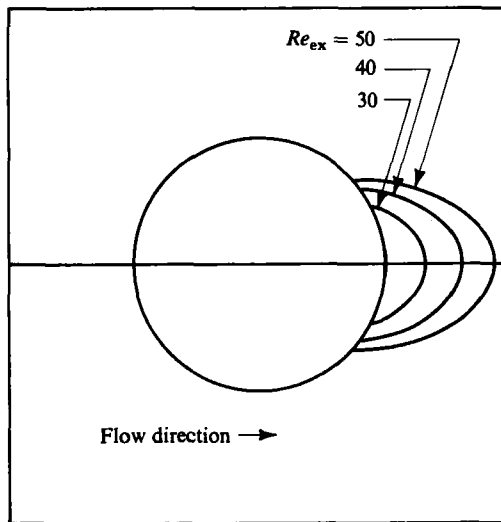


FIGURE 6. Boundaries of the recirculation region ($\psi = 0$), $X = 10^7$ for comparison with the experimental work of Taneda (1956).

$Re = 30$		$Re = 40$		$Re = 50$	
Present	Taneda	Present	Taneda	Present	Taneda
$r = 0.32$	≈ 0.32	0.68	≈ 0.61	0.965	≈ 0.87

TABLE 4. Comparison of the location of the rear end of the wake as predicted by the present solution and as interpolated from the experimental data of Taneda (1956)

Re X	0.5	1.0	2.0	5.0	10.0	20.0	50.0
0	33.8 (33.8)	17.5 (17.6)	9.3 (9.4)	4.25 (4.33)	2.43 (2.48)	1.41 (1.43)	0.69 (0.70)
0.333	38.3 (38.2)	19.9 (20.0)	10.6 (10.8)	4.89 (5.02)	2.87 (2.94)	1.71 (1.74)	0.89 (0.90)
1.0	42.9 (42.7)	22.4 (22.5)	12.1 (12.2)	5.65 (5.75)	3.33 (3.43)	2.05 (2.09)	1.12 (1.15)
3.0	47.4 (47.2)	24.8 (25.0)	13.4 (13.6)	6.36 (6.50)	3.80 (3.93)	2.38 (2.45)	1.36 (1.44)
Solid sphere	52.2 (51.8)	27.4 (27.5)	14.7 (15.1)	7.05 (7.28)	4.28 (4.45)	2.71 (2.81)	1.58 (1.72)

TABLE 5. Drag coefficients; Rivkind *et al.* (1976) ($Re_{ex} = Re_{in}$), present results in parentheses

Re_{ex}	10.0	20.0	50.0
Experimental results of Elzinga & Banhero (1961)	4.5	2.8	1.65
Rivkind <i>et al.</i> (1976)	4.28	2.71	1.58
Present results	4.45	2.81	1.72

TABLE 6. Comparison of drag coefficients for solid spheres

literature. Reasons for this wide range include droplet deformation and oscillation at larger velocities (Klee & Treyball 1956) and system impurities (Bachhuber & Sanford 1974). Thus experimental verification of a model based on comparison of drag coefficients alone is tenuous. However, since the drag coefficient is a parameter that is often measured in experimental studies, the experimental and numerical estimations of the drag coefficients of Abdel-Alim & Hamielec (1975) are compared with the present model in table 7. For comparison with the results of Abdel-Alim & Hamielec (1975), the interior Reynolds number was set such that $Re_{in} = Re_{ex}/X$ corresponds closely to their assumptions of nearly equal fluid densities.

There are significant differences between the theoretical drag coefficients predicted by Abdel-Alim & Hamielec (1975) and the present results. The exact cause of these discrepancies is not certain. It is possible that the free-stream conditions were imposed at a radius that was not sufficiently long to remove any significant end effects. The position at which the free stream was imposed by Abdel-Alim & Hamielec (1975) was not explicitly given. It may be estimated from the mesh dimensions that they range from about $r_\infty = 25.8$ for $Re = 1.0$ to $r_\infty = 7.4$ for $Re_{ex} = 50$. For the present study the free-stream conditions were imposed at $r_\infty = 300$. The predictive equation proposed by Abdel-Alim & Hamielec (1975) also appears to be questionable when compared with their own experimental and numerical predictions. For example, their predictive equation for the drag coefficient yields a drag coefficient of 4.00 for $Re_{ex} = 5.0$, $X = 0.0995$. Their numerically calculated drag coefficient was 4.39. For comparison it is seen that the predictive equation of Rivkind *et al.* (1976), predicts a drag coefficient of 4.51 and the present series-truncation method predicts a drag coefficient of 4.57. Other such examples may be obtained by comparing the values in table 7(a, c).

In the light of the good agreement between the present results and the predictive equation for drag coefficients proposed in Rivkind *et al.* (1976) (for $2.0 \leq Re_{ex} \leq 20.0$) and the discrepancies between the present results and the predictive equation of

(a) Abdel-Alim & Hamielec (1975) – calculated						
Re_{ex}	X	1.0	5.0	10.0	25.0	50.0
0.0995	17.5	4.39	2.50	—	—	—
0.301	19.2	4.81	2.89	—	—	—
0.554	20.0	5.12	3.11	—	—	—
0.266	—	4.54	—	1.31	0.84	—
0.708	—	4.90	—	1.60	1.11	—
1.40	—	5.02	—	1.69	1.23	—

(b) Abdel-Alim & Hamielec (1975) – experimental						
Re_{ex}	X	1.0	5.0	10.0	25.0	50.0
0.0995	18	4.6	2.8	—	—	—
0.301	19	5.0	3.1	—	—	—
0.554	20	5.2	3.3	—	—	—
0.266	—	4.5	—	1.45	0.9	—
0.708	—	4.9	—	1.75	1.2	—
1.40	—	5.0	—	1.8	1.25	—

(c) Present results ($Re_{in} = Re_{ex}/X$)							
Re_{ex}	n_0	X	1.0	5.0	10.0	25.0	50.0
0.0995	6	18.5	4.57	2.64	—	—	—
0.301	6	19.9	4.97	2.91	—	—	—
0.554	6	21.1	5.33	3.14	—	—	—
0.266	—	—	4.91	—	1.43	0.85	—
0.708	—	—	5.50	—	1.69	1.05	—
1.40	—	—	6.00	—	1.91	1.24	—

TABLE 7. Comparison of experimental (a) and numerical (b) estimations of the drag coefficient by Abdel-Alim & Hamielec (1975) with the present results (c)

Abdel-Alim & Hamielec (1975), the latter appears to be questionable. For $2.0 \leq Re_{ex} \leq 50.0$, the predictive equation of Rivkind *et al.* (1976) is recommended:

$$C_d = \frac{1}{1+X} \left[X \left(\frac{24}{Re_{ex}} + 4 Re_{ex}^{-\frac{1}{2}} \right) + 14.9 Re_{ex}^{-0.78} \right]. \quad (32)$$

Neither of the proposed predictive equations is adequate for low Reynolds numbers. As mentioned previously, the above equation does not work for Reynolds numbers smaller than 2, when it fails to converge to the creeping-flow solution for $Re_{ex} \rightarrow 0$. For $Re_{ex} < 2$ the predictive equation proposed in Oliver & Chung (1985) as given below should be used:

$$C_d = C_{d_{cf}} + 0.40 \left(\frac{3X+2}{X+1} \right)^2, \quad (33)$$

where $C_{d_{cf}}$ is the drag coefficient for creeping flow,

$$C_{d_{cf}} = \frac{8}{Re_{ex}} \left(\frac{3X+2}{X+1} \right). \quad (34)$$

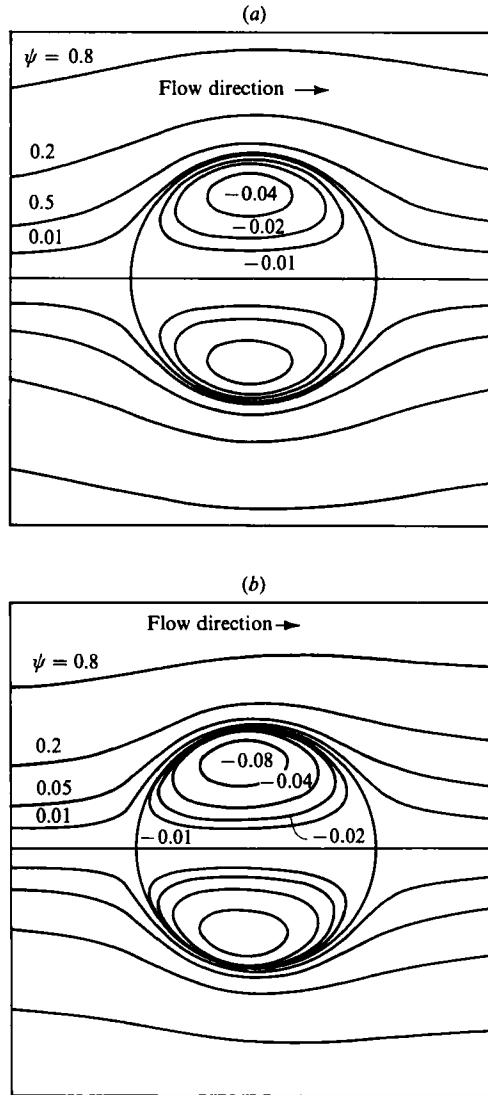


FIGURE 7. Stream-function contours for $X = 0.33$: (a) $Re_{ex} = 1.0$; (b) 50.0.

For a fluid sphere, as the Reynolds number increases, the internal circulation increases with the Reynolds number. This increased circulation is driven by the sharp velocity gradient near the droplet interface. This increased circulation is evident in figures 7(a, b) and 8(a, b), where the streamline contours are plotted for $Re_{ex} = 1$ and 50 for the viscosity ratios of $X = 0.333$ and 3.0 respectively.

This increased circulation inside the droplet may also be seen in the velocity profiles for the interfacial ($r = 1$) velocities (figure 9a, b). As the Reynolds number increases, the peak interfacial velocity increases. In addition, the symmetry about the $\theta = \frac{1}{2}\pi$ axis is lost. This increasing internal circulation will have effects on the rate of heat or mass transfer from the droplet.

Nakano & Tien (1967) used a Galerkin treatment to investigate the effects of the interior Reynolds number on the drag coefficient and on the interior circulation

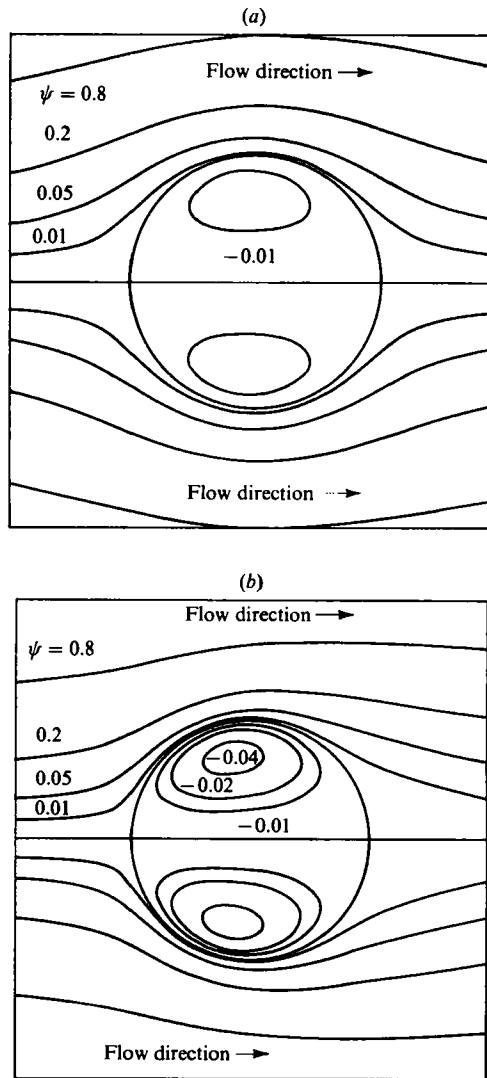


FIGURE 8. Stream-function contours for $X = 3.0$: (a) $Re_{ex} = 1.0$; (b) 50.0.

patterns. For the cases investigated, they found that the interior Reynolds number has an insignificant effect on the drag coefficient. However, their model predicted that the interior flow patterns were a function of the interior Reynolds number. This conclusion appears to contradict the work of Rivkind & Ryskin (1976). The Galerkin solution procedure used by Nakano & Tien (1967) employed very few trial functions and this produced results that were highly preliminary. For these reasons, a single simulation was made with the present method to compare the effects of the interior Reynolds number on both the drag coefficient and the droplet flow pattern. For this simulation a viscosity ratio of $X = 0.333$ was assumed with an interior Reynolds number of $Re_{in} = 200$ and an exterior Reynolds number of $Re_{ex} = 50$. The calculated drag coefficient for $Re_{in} = 200$, $Re_{ex} = 50$ was $C_d = 0.89$. This is about 1% lower than the drag coefficient ($C_d = 0.90$) for the same viscosity ratio and the exterior Reynolds number, but with an interior Reynolds number of $Re_{in} = 50$.

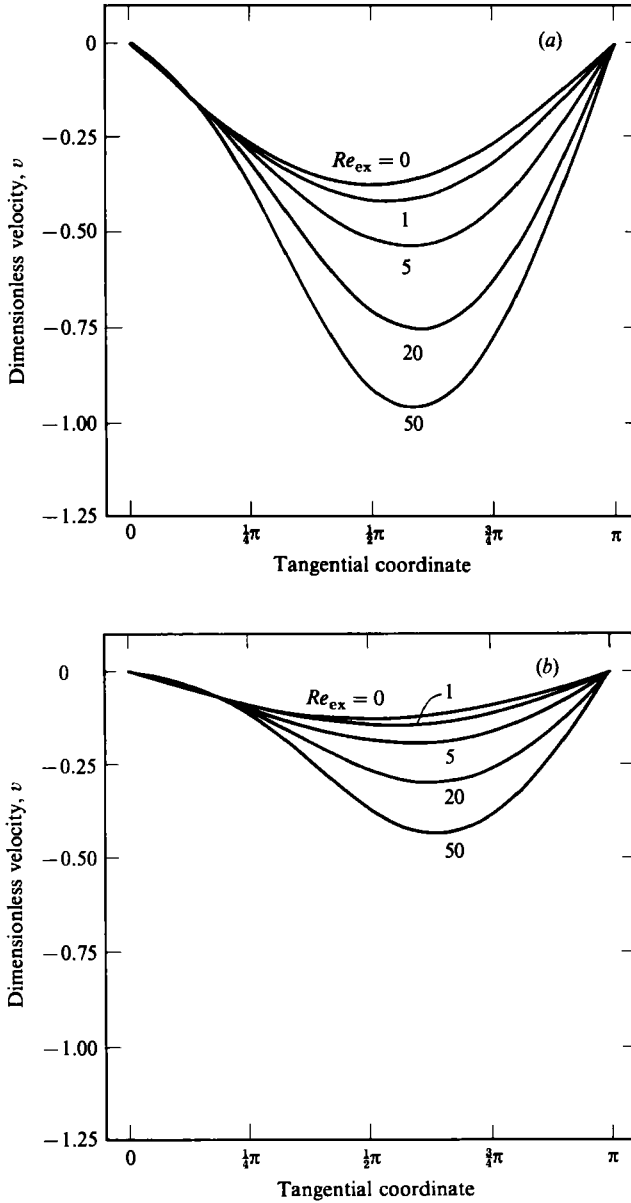


FIGURE 9. Tangential velocity at the interface for (a) $X = 0.333$; (b) 3.0.

The effects of the interior Reynolds number on the flow pattern have also been investigated. In figure 10, the interfacial velocity profiles have been plotted for these two cases. The interior Reynolds number was found to have only a limited effect on the interfacial velocities. A similar investigation was performed to investigate the effects of the interior Reynolds number on the flow pattern inside the droplet. Again it was not found to have a significant effect. Unless otherwise stated, the interior Reynolds number was set equal to the exterior Reynolds number as an input parameter for the present results.

Based on the conclusions of Rivkind *et al.* (1976) and the above investigation, it

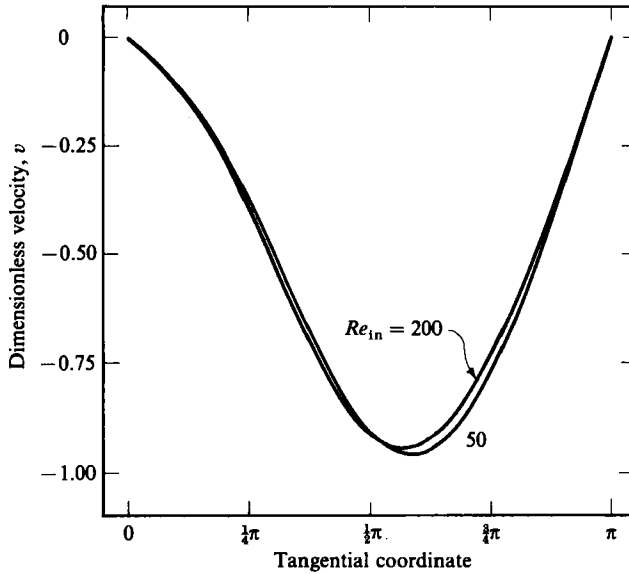


FIGURE 10. Tangential velocity at the interface as a function of Re_{in} for $Re_{ex} = 50.0$, $X = 0.333$.

may be assumed that for moderate interior Reynolds numbers with $Re_{ex} < 50$, the interior flow patterns and the drag coefficients are generally insensitive to changes in the interior Reynolds numbers.

5. Conclusion

The Navier–Stokes equations for steady axisymmetrical flow about a fluid sphere have been solved for moderate Reynolds numbers ($0.5 \leq Re_{ex} \leq 50$) using a coupled finite-element and series-truncation scheme. The present results agree closely with limited experimental measurements and also compare favourably with the finite-difference prediction of Rivkind *et al.* (1976). It was found that the equation proposed by Rivkind & Ryskin (1976) for predicting the drag coefficient was in good agreement with the present calculations for $2 \leq Re_{ex} \leq 20$. Based on our numerical results, an equation was proposed to predict the theoretical drag coefficient for low but finite Reynolds numbers between 0 and 2.

The strengths of the internal circulation were discovered to increase with Reynolds number. As the Reynolds number increases, the angle at which the wake recirculation begins also increases and the length of the recirculation region expands.

The present results did not compare favourably with the numerical results of Abdel-Alim & Hamielec (1975). It is proposed that the limited radius at which the free-stream conditions were imposed in that work may account for the errors in their results.

The conclusion drawn by Rivkind & Ryskin (1976), that for moderate Reynolds numbers (both interior and exterior) the flow patterns are often insensitive to the interior Reynolds number, was also confirmed in our numerical experiment.

REFERENCES

- ABDEL-ALIM, A. H. & HAMIELEC, A. E. 1975 *Ind. Engng Chem. Fund.* **14**, 308.
- BACHHUBER, C. & SANFORD, C. 1974 *J. Appl. Phys.* **45**, 2567.
- BRABSTON, D. C. & KELLER, H. B. 1975 *J. Fluid Mech.* **69**, 179.
- CLIFT, R., GRACE, J. R. & WEBER, M. E. 1978 *Bubbles, Drops and Particles*, Chaps 3 and 5. Academic.
- DENNIS, S. C. R. & WALKER, J. D. A. 1971 *J. Fluid Mech.* **48**, 771.
- ELZINGA, E. R. & BANCHERO, J. T. 1961 *AIChE J.* **7**, 394.
- HADAMARD, J. 1911 *C. R. Acad. Sci.* **152**, 1735.
- HUEBNER, K. H. 1975 *The Finite Element Method for Engineers*. Wiley.
- KLEE, A. J. & TREYBALL, R. E. 1956 *AIChE J.* **2**, 444.
- LECLAIR, B. P., HAMIELEC, A. E., PRUPPACHER, H. R. & HALL, W. D. 1972 *J. Atmos. Sci.* **29**, 728.
- NAKANO, Y. & TIEN, C. 1967 *Can. J. Chem. Engng* **45**, 135.
- OLIVER, D. L. R. & CHUNG, J. N. 1985 *J. Fluid Mech.* **154**, 215.
- RIVKIND, V. YA. & RYSKIN, G. M. 1976 *Fluid Dyn.* **11**, 5.
- RIVKIND, V. YA., RYSKIN, G. M. & FISHBEIN, G. A. 1976 *Appl. Math. Mech.* **40**, 687.
- ROTTENBERG, M., BIVINS, R., METROPOLIS, N. & WOOTEN, J. K. 1959 *The 3-J and 6-J Symbols*. MIT, Cambridge: The Technology Press.
- RYBCZNSKI, W. 1911 *Bull. Intl Acad. Pol. Sci. Lett. Cl. Sci. Math. Natur.* **A**, 40.
- TALMAN, J. D. 1968 *Special Functions*. Benjamin.
- TANEDA, S. 1956 *J. Phys. Soc. Japan* **11**, 1101.